Preprint, accepted for publication in the Proceedings of the Combustion Institute, July 2022. Presented at the 39th International Symposium on Combustion, Vancouver, BC Canada, 28 July 2022. Published version available at https://doi.org/10.1016/j.proci.2022.07.116

Ignition of Hexane-air Mixtures by Highly Under-expanded Hot Jets

Yunliang Qi, Joseph E. Shepherd*

Graduate Aerospace Laboratories, California Institute of Technology, 1200 E. California Blvd., Pasadena, California, 91125, United States

---

Abstract

We report an experimental study of ignition of flammable mixtures by highly unexpanded, supersonic hot jets. The high-pressure, hot-gas reservoir supplying the jet is created by impacting a projectile on a plunger to rapidly compress and ignite a rich n-hexane/air mixture, resulting in a peak reservoir pressure of more than 20 MPa. A locking mechanism was used to prevent the plunger from rebounding and the jet was created by rupturing a diaphragm covering a nozzle with an exit diameter between 0.25 and 1 mm. The jet development and ignition processes in the main chamber filled with hexane-air mixture were visualized using high-speed schlieren and OH* chemiluminescence imaging. The ignition threshold was determined as a function of composition in the jet and main chamber, the nozzle diameter, and the initial pressure in the main chamber. Unlike the case of subsonic jets in which ignition occurs at the shear layer near the nozzle exit, ignition of combustion in the main chamber was found to take place downstream of the Mach disk terminating the supersonic expansion and within the turbulent mixing region created by the startup of the supersonic jet. The results are interpreted using a constant-pressure, well-stirred reactor model simulating the mixing between the hot jet and cold ambient gas. The critical conditions for ignition are determined by the competition between energy release due to chemical reactions initiated by the hot jet gas and cooling due to mixing with the cold chamber atmosphere. The critical value (maximum for which ignition occurs) of the mixing rate was computed using a detailed chemical reaction model and found to be a useful qualitative guide to our observations.

Keywords: Highly under-expanded jet; Ignition; Rapid compression; Visualization; Mixing rate

---

*Corresponding author: joseph.e.shepherd@caltech.edu.

1. Introduction

On average a commercial airliner is struck by lightning once a year [1]. When a lightning strike attaches to a metallic fastener on the wing, Joule heating by the high current between the fastener and underside of the wing surface can vaporize metal and composite materials to create the jets of hot gas and particles emerging from underneath the fastener into the fuel tank. Ignition of flammable mixtures in the tank ullage by these hot jets and particles are a potential hazard that must be considered in airframe design and manufacture [1-3].

Ignition by hot gas jets has long been an important topic in other areas, such as internal combustion engines [4, 5] and chemical process industry [6]. However, these studies on jet ignition have typically focused on low-speed jets created by modest pressure ratios (PR) between the jet reservoir and combustion chamber. The reservoir used to supply the hot jet is usually combustion products created by low-speed combustion in the reservoir chamber. For example, in internal combustion engine (ICE) applications, the maximum PR between the jet/pre-chamber and the main chamber is usually around two [5]. A widely used test in industrial hazard evaluation for jet ignition is the determination of the "Maximum Experimental Safe Gap" (MESG) [6]. The maximum PR between the test chamber and surrounding atmosphere in these tests is usually less than eight , the approximate maximum PR under constant-volume combustion conditions of nominal atmospheres.

In the present study, we are motivated to examine higher pressures by the issue of lightning strike on metallic fasteners in aircraft [2, 3]. Teulet et al. [3] estimated that the pressure within the affected region could be between 10 and 300 MPa. Considering that the ambient pressure in an aircraft fuel tank is 0.02 to 0.1 MPa, the PR between the high-pressure reservoir and the tank ullage is greater than 100. The lightning strike process is highly transient and following the lightning strike, the high-pressure gas will be vented as an under-expanded hot gas jet from a small volume. The pressure ratio and small dimensions of the jet make this situation quite different than previous jet ignition studies.

A related problem to jet ignition at very high pressure ratios is the "secondary flash" in gun muzzle flows [7]. At the time the projectile exits the muzzle, the pressure in the gun barrel can still be as high as 100 MPa [8]. The propellant gas leaving the muzzle forms a highly under-expanded jet and fresh air can be entrained into the jet downstream of the Mach disk. The mixing of the entrained air and the incomplete burnt species or residual propellant particles in the muzzle plume may cause ignition resulting in a "secondary flash" [7]. Although this process has been revealed in numerical simulations [9], experimental studies, especially by visualization, on the ignition process and the conditions under which ignition occurs are really rare.

The goal of our study was to experimentally examine the ignition by highly under-expanded hot jets with parameters relevant to the evaluation of lightning strike ignition hazards. To achieve these parameters, we had to develop a new experimental facility, and characterize the performance. With this facility, we then conducted a series of tests to examine the nature of the ignition processes in flammable atmospheres with hydrocarbon fuel-air mixtures.

2. Experimental setup

The experiments were performed in a specially designed fixture, shown in Fig. 1(a). The fixture had a jet chamber with a minimum volume of ≈1 mL and a main chamber of volume ≈0.68 L. The two chambers were connected through a single hole with length 1 mm, and diameter (D_n) that could be either 0.25, 0.5 mm, 0.75 mm or 1 mm, Fig. 1(b). The nozzle consisted of two parts between which an aluminum diaphragm (thickness (δ_d) = 12.7 to 76.2 μm) was clamped to separate the gases in the two chambers before an experiment started. To create a hot gas reservoir in the jet chamber, a gas gun was used to accelerate a steel projectile (3.571 kg) that impacted on a polycarbonate plunger (0.197 kg), rapidly compressing the gas in the jet chamber. The jet chamber had a step near its end to increase the compression ratio (CR), see Fig. 1(b). A piezoelectric pressure sensor (PCB 113B23) was used to measure the pressure in the jet chamber (p_{jc}).

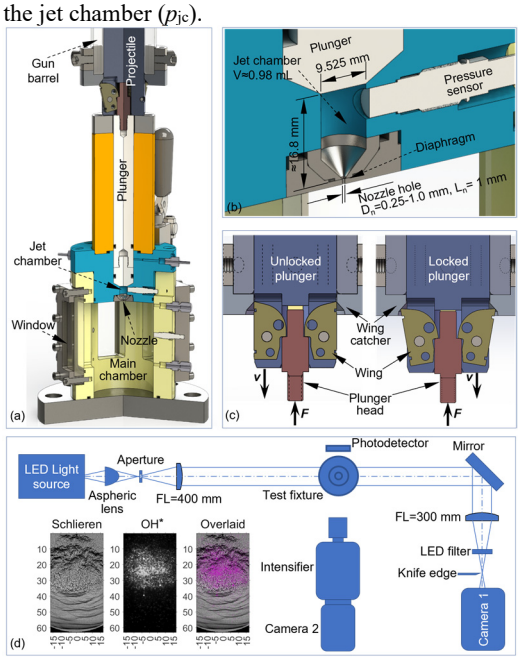

Fig. 1. Schematics of experimental setup. (a) test fixture; (b) jet chamber and nozzle; (c) plunger-locking mechanism; (d) optical setup

Although the gas gun is capable of driving a projectile to 200 m/s [10], to protect the polycarbonate plunger from damage by multiple high-speed impacts, we used a projectile velocity of around 6 m/s. When the plunger was about to reach the end of compression (EOC), four locking wings installed on the projectile were pushed out by the plunger and contact the aluminum wing catcher ring, Fig. 1(c). Through this mechanism, the plunger can be locked at the EOC. Otherwise, the rebound of the plunger will rapidly decrease the jet pressure and temperature.

Due to the high CR, the flammable mixture in the jet chamber would autoignite near the EOC. The increase in chamber pressure due to the combination of compression and autoignition will cause the diaphragm to rupture, initiating flow through the jet orifice. Depending on the conditions, rupture may occur either before or after autoignition. A photodetector (Thorlabs APD110A) and schlieren imaging was used to monitor the timing of diaphragm rupture and the chemiluminescence of the emerging gas jet. The subsequent jet development in the main chamber was visualized using a schlieren system with high-speed recording (Phantom V2512 camera operated at 140k to 250k fps) and simultaneous OH* chemiluminescence (300-320 nm spontaneous radiation due to transitions from A^2S^+ to X^2P states) in a perpendicular direction by an intensified camera (LaVison HS-IRO combined with a Phantom V7.3 camera operated at 19k fps), Fig. 1(d). The window size for both schlieren and OH* visualization was 35.6 × 77.5 mm. However, limited by the image resolution at high frame rates and other factors like lens diameter and magnification ratio, the visualized area was smaller than the window size and varied with specific experimental purposes. Although schlieren and OH* images are taken from different directions, the inset image in Fig. 1(d) shows that due to the approximate axial symmetry of the jet, the reacting region in the OH* image agrees well with the gas flow region in the schlieren image, which provides a convenient way to examine the ignition or extinction process. The pressure in the main chamber (p_{mc}) was measured by a piezoelectric (PCB 113B23) pressure sensor.

The cameras and data-acquisition were triggered by the rise in pressure in the jet chamber and recording of samples before the trigger was utilized to capture the entire event. The pressures and photodetector signals were recorded by a digital oscilloscope (Yokogawa DL850) sampling at 20 MHz.

Since we aimed to study ignition in the context of aviation, hexane (>99%) was used as a surrogate of jet fuel to make combustible mixtures with oxygen and nitrogen using the method of partial pressure. The molar ratio of nitrogen to oxygen was 3.76. When different equivalence ratios were needed for the jet chamber and the main chamber, the two mixtures were prepared separately in two stainless steel bottles (3.78 L). A recirculation pump was used for mixing. All experiments and preparations were done at room temperature (296±1 K). Unless specified, the initial pressure in the jet chamber and main chamber ($p_{0,jc}$ and $p_{0,mc}$) before compression were all 0.1 MPa. A plunger stroke of 90 mm was used for all the experiments, resulting in a CR of 47.

3. Experimental results

Experiments were initially performed to validate the effect of plunger locking on the ignition in both jet chamber and main chamber. Then the development of the hot gas jet and the ignition process in the main chamber were analyzed under representative conditions. Lastly, tests were conducted under different combinations of nozzle diameter (D_n) and equivalence ratios in the two chambers (φ_{jc} and φ_{mc}). The outcome of each test condition was observed to have intrinsic variability. Although we were not able to obtain sufficient data to conduct a statistical analysis, we were able to bracket the ignition thresholds though repetition of tests. For each combination of D_n, φ_{jc} and φ_{mc}, the test was repeated at least three times. If ignition did not occur in the three shots, this combination would be considered as a no-ignition condition. Otherwise, it would be considered as an ignition condition no matter how many times ignition occurred.

3.1 Validation of plunger locking

Fig. 2 compares the effect of plunger locking on ignition in both the jet chamber and main chamber. For the unlocked case, the locking mechanism on the projectile was removed, and the resulting weight change was compensated by adding a steel block. It can be seen in Fig. 2(a) and (b) that, when the locking mechanism is installed, the plunger almost moves together with the projectile at the same velocity during the late stage of compression. The spike in the plunger velocity trace right before EOC (around t=17 ms, see the blue line in the locked case in Fig. 2(b)) is due to the plunger's upward movement relative to the projectile when the locking wings are being pushed out (see Fig. 1(c)). After being fully pushed out, the locking wings can clamp the plunger, so the plunger will move together with the projectile again and finally be locked at the EOC after the locking wings are caught by the wing catcher. In contrast, when the locking mechanism is removed, although the plunger can reach a higher velocity (10.7 m/s vs. 8.6 m/s) from the direct impact by the projectile, it will experience multiple rebounds. Comparing with the locked case, the rebound immediately before EOC causes a lower first peak combustion pressure ($p_{p1,}$ 20.6 MPa vs. 40.9 MPa) and a lower diaphragm rupture pressure ($p_{r,}$ 22.0 MPa vs. 27.8 MPa), as shown in Fig. 2 (c) (p_{p1} and p_r are marked by the blue and black arrows, respectively). At the time of diaphragm rupture, the projectile has not reached the EOC and will impact the plunger again, so the combustion products in the jet chamber can be compressed to a higher maximum pressure (p_{max}) than the locked case, 59.9 MPa vs.

55.3 MPa. However, even with a higher p_{max}, ignition in the main chamber does not occur for the unlocked case, see Fig. 2(d). This suggests that the diaphragm rupture pressure (p_r) has a more decisive influence on the ignition in the main chamber than the p_{max} in the jet chamber does. In summary, to obtain a higher p_r, the plunger has to be locked at the EOC, and the locking mechanism was successfully used in all ignition tests.

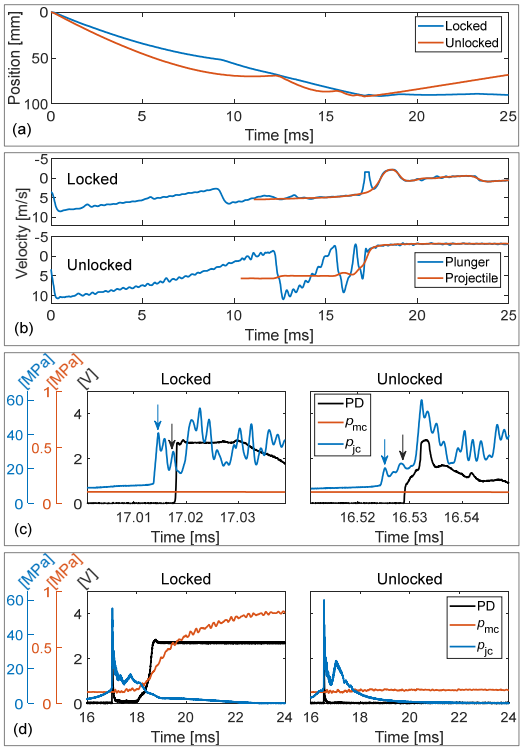

Fig. 2. Effect of plunger locking on ignition in both the jet chamber and main chamber (φ_{jc}=2, φ_{mc}=1, D_n=1 mm, δ_d=50.8 μm). (a) plunger movement; (b) velocities of plunger and projectile; (c) zoom-in views of pressure traces and photodetector signal, blue arrows denote the first peak pressure (p_{P1}) after ignition, black arrows denote the diaphragm rupture pressure (p_r); (d) pressure traces and photodetector signal in a longer time range.

3.2 Development of the highly under-expanded hot jet and ignition process in the main chamber

The characteristic features, e.g., barrel shocks, primary vortex ring and Mach disk, of an under-expanded supersonic jet are observable within 0.020 ms of diaphragm rupture. Due to the large density difference and high-level of turbulence, these features are difficult to visualize in the initial stage of jet formation when the jet chamber ignites before diaphragm rupture. By reducing the diaphragm thickness and enabling rupture before ignition in the jet chamber, these features can be clearly observed in Fig. 3. Once the jet chamber ignites, these features are obscured by strong density fluctuations, as in the 0.220 ms image of Fig. 3. For the data presented in the subsequent sections of this paper, results are shown only for cases when the diaphragm ruptures after the jet chamber ignites.

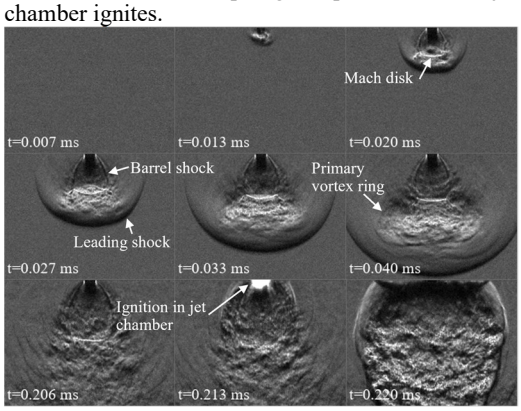

Fig. 3. A close-up view of the development of a jet created before the jet chamber ignites (D_n=1 mm, φ_{jc}=2, φ_{mc}=0 (air), δ_d=25.4 μm, visualized area=21×16 mm^2).

The development of the jet and ignition processes with different nozzle diameters were qualitatively similar. To observe more fully the jet development and ignition process, the imaging system magnification was reduced so that the field of view was 33×63 mm. A representative ignition process with D_n = 0.5 mm is presented in Fig. 4. The images from the schlieren and OH* system have been synchronized and overlaid using purple false color for the OH* signals.

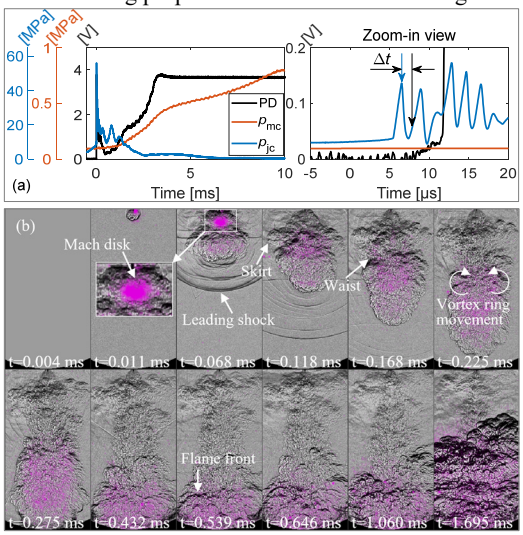

Fig. 4. A representative ignition process in the main chamber under D_n=0.5 mm (φ_{jc}=2, φ_{mc}=1, δ_d=25.4 μm, visualized area=33×63 mm^2). (a) pressure traces and photodetector signal; (b) schlieren images overlaid with OH* chemiluminescence.

As shown in Fig. 4(a), the diaphragm ruptures at around 0.0079 ms at p_r = 19.6 MPa (marked by the black arrow in the zoom-in view of the pressure trace). Although the pressure oscillates with large amplitudes

after the diaphragm ruptures, the lowest pressure is still higher than 8.9 MPa, creating a highly under-expanded jet with an initial velocity exceeding 1000 m/s.

The jet gas cools as it expands to low pressure, and the chemical reactions are predicted to be rapidly quenched in the region between the nozzle and the Mach disk. The pressure and temperature increase across the Mach disk, resulting in the resumption of chemical reactions downstream. Evidence of this is shown in the image at 0.068 ms, with a bright OH* signal visible just downstream from the position of the Mach disk.

An obvious jet "skirt" near the nozzle is formed after 0.118 ms. With increasing time, the jet penetrates in the combustion chamber and a distinct narrowing or "waist" appears downstream of the Mach disk. The jet velocity is estimated to be less than 300 m/s after passing through the Mach disk. The velocity continues to decrease downstream due to the momentum exchange through entrainment of the chamber gas into the primary vortex ring and the head of the jet. Because the temperature of the jet downstream of the Mach disk has recovered to close to that at the nozzle exit, the entrainment-induced mixing between the hot jet and the fresh mixture can lead to reactions when the mixed gas has a sufficiently high temperature. This appears to be the key mechanism for ignition of combustion in the chamber gas.

After 0.168 ms in Fig. 4, significant OH* radical emission is observed from the downstream portion of the jet. At 0.539 ms, a flame front is observed to form and propagate upward to the nozzle. Up to this time, the chamber pressure p_{mc} has remained close to the initial value. As flame propagation proceeds, p_{mc} is observed to increase, reaching approximately the constant volume, adiabatic combustion value in about 10 ms. This ignition process starting from the jet head at high PRs is similar to those observed under low PRs with ICE relevant conditions [11, 12].

3.3 Influence of diaphragm rupture on repeatability

Tests like those shown in Fig. 4 usually resulted in ignition. However, ignition did not always occur under the same nominal conditions in every test. Even when a larger nozzle diameter was used, occurrence of ignition was uncertain. Fig. 5 shows a no-ignition event with D_n = 1 mm. The OH* signals are still quite strong at the initial stage. However, as the time elapses and the cold gas keeps being entrained into the jet, the OH* signals become weaker and finally disappear as ignition fails. We repeated the tests with D_n = 1 mm seven times with the same mixture; six ignitions and one no-ignition were obtained.

The difference in ignition and no-ignition cases is correlated with the time difference Δt shown in Fig. 6(a), between p_{pl} and p_r. As shown in Fig. 6(a), the no-ignition case has the longest Δt. A longer Δt means more heat loss to the wall, resulting in a lower jet temperature. The value of Δt was observed to be influenced by the clamping pressure on the diaphragm and construction of the split nozzle. As shown in Fig. 6(b), the diaphragm used in the ignition case has a more obvious indentation mark made by the split nozzle than that used for the no-ignition case. The effective diaphragm thickness becomes smaller, and it will be broken more easily and earlier. No-ignition was also observed when the diaphragm ruptured much earlier before the jet chamber ignites. In subsequent tests, the diaphragm thickness and clamping pressure were adjusted and test results with consistent values of Δt were used in evaluating ignition thresholds.

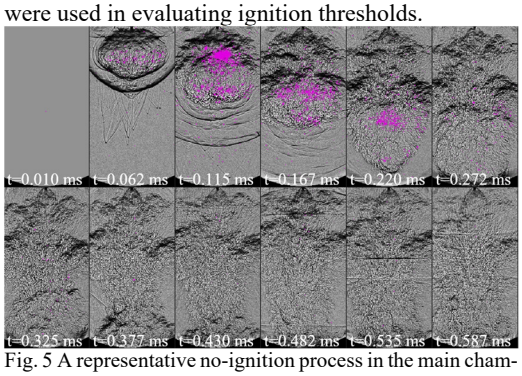

Fig. 5 A representative no-ignition process in the main chamber under D_n=1 mm (φ_{jc}=2, φ_{mc}=1, δ_d=50.8 μm, visualized area=33×63 mm^2, OH* signals are four times enhanced).

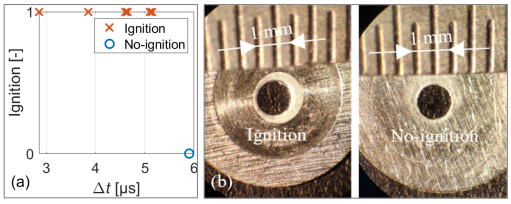

Fig. 6. Effect of diaphragm rupture on ignition (φ_{jc}=2, φ_{mc}=1, δ_d=76.2 μm). (a) ignition as a function of Δt; (b) microscopic images of diaphragms under ignition and no-ignition.

3.4 Effect of equivalence ratio and nozzle diameter

Given that the ignition takes place downstream of the Mach disk in subsonic flow, we propose that ignition is governed by the same criteria as used by Malé et al. [13] for subsonic jets. They found that ignition was characterized by a critical mixing rate $\theta_c \sim U_{jet}/D_{jet}$, where U_{jet} and D_{jet} are the characteristic diameter and exit velocity of the jet. Ignition is only possible if $\theta < \theta_c$ so that chemical reactions can effectively compete with the cooling effect of mixing.

In application to highly under-expanded jets, we propose replacing the jet exit parameters with the conditions just downstream of the Mach disk so that $\theta_c \sim U_{Mach}/D_{Mach}$. All other factors being the same, the diameter of the Mach disk D_{Mach} is proportional to the nozzle diameter so we expect to see an effect of nozzle diameter like that observed in subsonic jets. We

anticipate that the main influence on ignition other than jet diameter will be the jet temperature and composition as well as the reactivity of the combustion chamber mixture.

Three equivalence ratios, 0.5, 1 and 2, were examined for both the jet chamber (φ_{jc}) and main chamber (φ_{mc}) using four nozzle diameters D_n = 0.25, 0.5, 0.75 and 1 mm. To make sure that the diaphragm ruptured after the jet chamber ignites and the time Δt was not too large, diaphragm thicknesses of δ_d = 12.7, 25.4, 50.8 and 76.2 μm were used for the four nozzles, respectively. Fig. 7(a) shows the results. For D_n = 0.25 mm, ignition does not occur for any conditions. For the other three D_n values, ignition can only occur at φ_{jc} = 2 and φ_{mc} = 1.

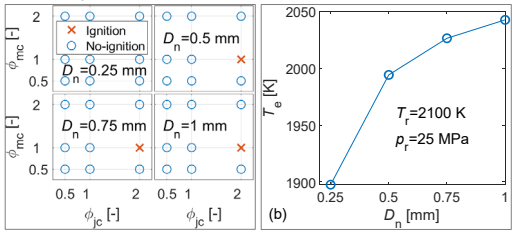

Fig. 7. Ignition for different equivalence ratios and D_n. (a) test matrix; (b) T_e as a function of D_n

We propose that the explanation of why ignition occurs only for φ_{jc}=2 is due to the hot CO and H_2 in the combustion products of the rich mixture. The combustion of these fuels will enhance energy release and promote ignition as the jet mixes with the flammable mixture in the combustion chamber. When the combustion chamber mixture is too rich or too lean, the opposite effect occurs. The ignition delay time of the mixed gas will be higher and the energy release less than for the stoichiometric mixtures, inhibiting ignition.

In addition to the effect on the Mach disk diameter, the nozzle diameter D_n will influence the jet temperature at the nozzle exit (T_e). T_e is lower than the temperature at diaphragm rupture (T_r) due to the heat loss to the wall when the jet flows through the nozzle. Fig. 7(b) shows the variation of T_e as a function of D_n, which was estimated using the empirical correlations provided in Malé et al. [14] and assuming the same values of T_r = 2100 K and p_r = 25 MPa for the four nozzles. T_e decreases with decreasing D_n. Changing D_n from 1 mm to 0.5 mm, T_e decreases by 48 K. However, as D_n further decreases from 0.5 mm to 0.25 mm, T_e decreases by 97 K to nearly 1900 K. This decrease in temperature will be reflected in a decrease of temperature downstream of the Mach disk, potentially inhibiting the ignition process.

3.5 *Effect of initial pressure*

The effect of initial pressure was examined for the main chamber ($p_{0,mc}$) over a range from 0.04 to 0.2 MPa with φ_{jc} = 2 and φ_{mc} = 1. The results are summarized in Fig. 8. Generally, the lower limit of $p_{0,mc}$ for ignition increases with the decrease of D_n. For D_n = 1, 0.75 and 0.5 mm, the lower limits of $p_{0,mc}$ are 0.07, 0.07 and 0.08 MPa, respectively. The ignition processes visualized at these pressures are similar to those shown in Fig. 4(b).

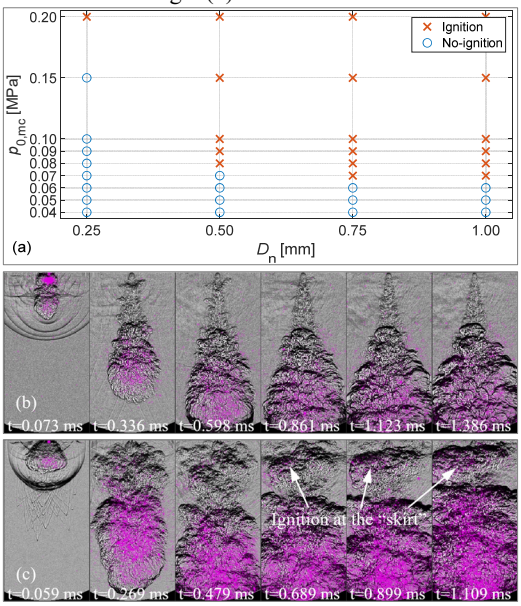

Fig. 8. Ignition for various values of $p_{0,mc}$ and D_n (φ_{jc} = 2, φ_{mc} = 1). (a) test results; (b) ignition process for $p_{0,mc}$ = 0.2 MPa and D_n = 0.25 mm; (c) ignition process for $p_{0,mc}$ = 0.2 MPa and D_n = 0.75 mm.

For D_n = 0.25 mm, due to its lower T_e compared with the other three nozzles, ignition can only occur when $p_{0,mc}$ is increased to 0.2 MPa. Fig. 8(b) shows an ignition process for D_n = 0.25 mm, in which the ignition occurs at the jet head, as in Fig. 4(b). However, with larger nozzle diameters at higher $p_{0,mc}$, ignition could occur at the "skirt" independently near the nozzle in addition to the jet head, as shown in Fig. 8(c) for D_n = 0.75 mm and $p_{0,mc}$ = 0.2 MPa.

Due to the lower PR, there was no obvious "skirt" structure in the jet in previous ICE and MESG related jet ignition studies [15-17]. Ignition near the nozzle exit in those studies is usually caused by flame propagation from flame kernels far downstream of the nozzle exit or for low-speed jets, in the jet shear layer near the nozzle. In the present study, the "skirt" region also can entrain ambient fresh gas as it moves at a relatively low velocity, providing a possibility to ignite there. However, the temperature in this region is usually lower than that at the jet head [18], so the ignition is more difficult. As $p_{0,mc}$ increases, the expansion of the jet is suppressed and the ignition delay time of the mixed gas is shortened; thus, the ignition in this region becomes possible. The influence of $p_{0,mc}$ on the critical mixing rate for ignition will be discussed in the next section.

4. Modeling

The results presented in the above sections have shown that the ignition is associated with the mixing between the hot jet and the combustion chamber gas downstream of the Mach disk. The pressure p_{mc} in the chamber is essentially constant during the ignition period. These conditions are similar to those encountered in low-speed jet ignition [13, 14, 19] and we adopt the approach used by those researchers in modeling the ignition processes in the turbulent mixing region downstream of the Mach disk.

We approximate the ignition process as a time-dependent, well-stirred and constant-pressure reactor. The reactor is an open control volume and is initially filled with hot combustion products. The cold fresh mixture flows into the reactor and mixes with the hot combustion products, the mixed gas flows out of the reactor at the same rate. Following the approach of Malé et al. [13,14], the governing equations of the reactor can be written as functions of θ and ξ, where θ is the mixing rate calculated by the ratio of the incoming flow rate to the total mass in the reactor, and ξ is the mass fraction of the original hot combustion products in the reactor. For the closure relation $\theta(\xi)$, we adopt the approximation of Malé et al. [13,14] who proposed on the basis of DNS results that $\theta = \theta_0 4\xi(1-\xi)$, where θ_0 is the initial maximum mixing rate. Cantera and MATLAB were used to solve the reactor equations with a previously validated detailed reaction mechanism [20] for hexane.

Fig. 9 shows an example of calculated temperature evolution as a function of time or mixture fraction ξ for several values of θ_0. The initial hot gas in the reactor is the combustion products of the jet chamber with $\varphi_{jc} = 2$. The composition and initial temperature ($T_{0,R}$, 2100 K) are estimated by assuming constant-volume combustion in the jet reservoir followed by isentropic expansion and a shock wave (simulating the Mach disk) with downstream pressure equal to the reactor initial pressure ($p_{0,R}$) of 0.1 MPa. The entrained chamber mixture has an equivalence ratio (φ_{mc}) of 1 and a temperature ($T_{0,in}$) of 296 K. For values of θ_0 less than critical ones $\theta_{0,c}$, ignition takes place and ξ drops from 1 to nearly zero within 1 ms, consistent with observations in our experiments (Fig. 4 and Fig. 5). Larger values of θ_0 correspond to higher values of entrainment rates of the cold chamber gas. For $\theta_0 > \theta_{0,c}$, the hot gas fraction (ξ) and mixture temperature decreases sufficiently rapidly during mixing that the energy release by the chemical reactions in the mixed gas is not able to balance the cooling, and ignition does not occur. In those cases, the temperature will decrease until it reaches $T_{0,in}$ when the reactor is fully occupied by cold gas, i.e., ξ=0, as shown in Fig. 9(b) and consistent with the results obtained in Ref. [13, 14, 19] because the same basic models are used in the present study as in theirs. For near-critical values of θ_0, the temperature initially decreases with increasing mixture fraction or time, and, if ignition is possible, the temperature will subsequently increase until it reaches the equilibrium temperature.

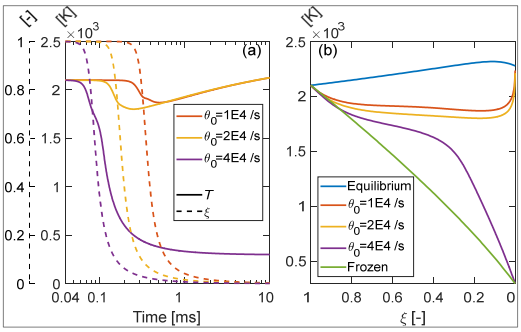

Fig. 9. Evolution of the parameters of the open reactor ($T_{0,R}$=2100 K, $p_{0,R}$=0.1 MPa, $T_{0,in}$=296 K). (a) temperature and ξ evolution as a function of time with different values of θ_0; (b) temperature evolution as a function of ξ with different values of θ_0, the equilibrium and frozen lines represent the cases with $\theta_0 \to 0$ and $\theta_0 \to \infty$, respectively.

A map or diagram of the regimes of ignition and no-ignition is obtained by graphing the results of reactor simulations over a grid of values for jet and combustion chamber conditions as a function of the mixing parameter θ_0.

Fig. 10(a) shows an example ignition map for $T_{0,R}$ and θ_0 with $\varphi_{jc} = 2$, $\varphi_{mc} = 1$, $T_{0,in} = 296$ K and $p_{0,R} = 0.1$ MPa. A nearly linear boundary can be seen between the ignition and no-ignition cases. The critical value $\theta_{0,c}$ as a function of $T_{0,R}$ was determined by logistic regression and plotted in Fig. 10(b) for various values of φ_{jc} and φ_{mc}. Among the cases examined, when $T_{0,R}$>1700 K, the combination of φ_{jc}=2 and φ_{mc}=1 has the highest value of $\theta_{0,c}$, which means the most likely ignition. This is consistent with the experimental results shown in Fig. 7.

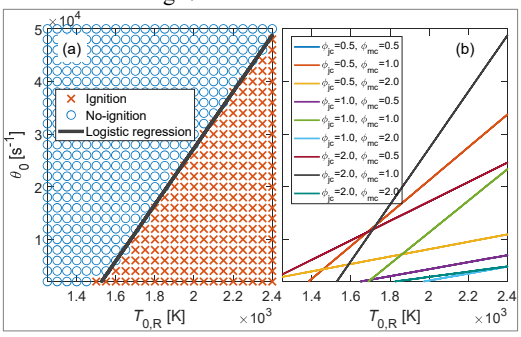

Fig. 10. Effect of $T_{0,R}$, θ_0 and equivalence ratio on ignition ($T_{0,in}$=296 K, $p_{0,R}$=0.1 MPa). (a) ignition map under different $T_{0,R}$ and θ_0; (b) variation of critical θ_0 with φ_{jc} and φ_{mc}, the line of φ_{jc}=0.5 and φ_{mc}=0.5 overlaps with the line of φ_{jc}=1.0 and φ_{mc}=0.5.

The effect of varying the initial reactor pressure $p_{0,R}$ is shown in Fig. 11(a). The value of $\theta_{0,c}$ increases with increasing $p_{0,R}$ at a given jet temperature. There are two possible explanations. One is that as $p_{0,R}$ increases, the jet velocity will decrease, causing $\theta_{0,c}$ to decrease and ignition becomes more likely [13]. Another is that the reactivity (as measured by ignition delay time) of the chamber mixture will increase in

proportion to pressure, resulting in higher values of $\theta_{0,c}$ at higher $p_{0,R}$. The combined effect of these factors makes ignition more likely to occur under higher $p_{0,R}$. We speculate that this also enables ignition within the "skirt" region at lower temperature and velocity as suggested by [18]. Fig. 11(b) shows the values of $\theta_{0,c}$ as a function of $p_{0,R}$ for three values of $T_{0,R}$. All the cases exhibit nearly linear variation of $\theta_{0,c}$ with $p_{0,R}$, indicating that the limiting reactions in the mixed gas are bimolecular so that the energy release and net reaction rates are proportional to pressure. This is consistent with the high-temperature reaction mechanism.

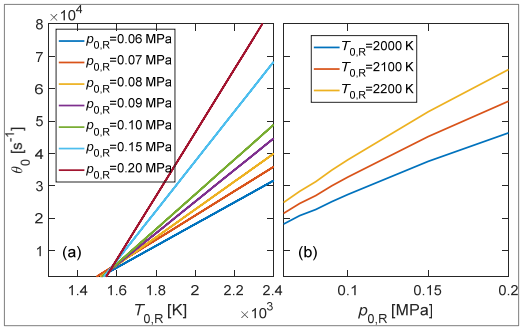

Fig. 11. Effect of $p_{0,R}$ on critical θ_0 ($T_{0,in}$=296 K, φ_{jc}=2, φ_{mc}=1). (a) variation of critical θ_0 with $p_{0,R}$ and $T_{0,R}$; (b) critical θ_0 as a function of $p_{0,R}$ under fixed $T_{0,R}$.

5. Conclusions

We developed and characterized an experimental facility to examine the ignition of hexane-air mixtures by highly under-expanded hot jets as a function of jet parameters and mixture conditions with pressure ratios across the nozzle larger than 200. High-speed schlieren and OH* chemiluminescence were used to visualize the jet development and ignition processes. A constant-pressure and well-stirred open reactor model was used to help understand the experimental results.

The pressure at the time of jet formation in the jet chamber had decisive influence on ignition in the main chamber because it determined the temperature of the jet head that would first mix with the flammable gas in the main chamber. The earlier the jet formed after the jet chamber ignited, the more likely the ignition would occur.

The combination of the fuel-rich mixture in the jet chamber and the stoichiometric mixture in the main chamber was most likely to cause ignition in the main chamber. We attribute this to the combustion of the rich combustion products, CO and H_2, in the hot jet and the low ignition delay time of the stoichiometric mixture.

The ability of the hot jet to cause ignition decreased as the nozzle diameter decreased from 1 mm to 0.25 mm and as the main chamber pressure decreased from 0.2 MPa to 0.04 MPa. When ignition occurred under low pressure ratios, the ignition starts from the jet head. At higher pressure ratios, the ignition could occur separately at both the jet head and the "skirt" region near the nozzle.

Numerical simulations with a stirred reaction model indicated that ignition in the main chamber can be explained by the competition between energy release due to chemical reactions and cooling due to mixing of the cold chamber gas within the turbulent mixing region downstream of the Mach disk. Ignition thresholds were characterized by computing the initial critical mixing rate for given jet and chamber conditions. The initial critical mixing rate was the highest under the combination of the fuel-rich mixture in the jet chamber and the stoichiometric mixture in the main chamber, and it increased with the initial jet temperature and main chamber pressure. This is in accordance with the trends observed in our experimental results.

More sophisticated analyses and numerical simulation of the compressible flow, mixing and chemical reaction processes will be required to make further progress in predicting critical conditions for ignition. Further refinement of the present experimental technique or development of alternative methods of hot gas get generation is needed in order to provide a data base for validating numerical simulations and engineering models used for lighting strike hazard evaluation.

Acknowledgement

This work was supported by The Boeing Company through a Strategic Research and Development Relationship Agreement CT-BA-GTA-1.

References

[1] A. Larsson, P. Lalande, A. Bondiou-Clergerie, A. Delannoy, The lightning swept stroke along an aircraft in flight. Part I: thermodynamic and electric properties of lightning arc channels, *J Phys D Appl Phys*, 33 (2000) 1866-1875.

[2] S. Evans, M. Jenkins, M. Cole, M. Haddad, D. Carr, D. Clark, C. Stone, A. Fay, R. Mills, D. Blair, L. Allgood, H. Hackford, An introduction to a new aerospace lightning direct effects research programme and the significance of Zone 2A waveform components on sparking joints, *33rd Int. Conf. Light. Prot.* (2016).

[3] P. Teulet, T. Billoux, Y. Cressault, M. Masquere, A. Gleizes, I. Revel, B. Lepetit, G. Peres, Energy balance and assessment of the pressure build-up around a bolt fastener due to sparking during a lightning impact, *Eur. Phys. J. Appl. Phys.*, 77 (2017) 20801.

[4] E. Toulson, H.J. Schock, W.P. Attard, A Review of Pre-Chamber Initiated Jet Ignition Combustion Systems, *SAE Technical Paper 2010-01-2263*(2010).

[5] S. Zhu, S. Akehurst, A. Lewis, H. Yuan, A review of the pre-chamber ignition system applied on future low-carbon spark ignition engines, *Renew. Sust. Energ. Rev.*, 154 (2022) 111872.

[6] P. Thibault, Y.K. Liu, C. Chan, J.H. Lee, R. Knystautas, C. Guirao, B. Hjertager, K. Fuhre, Transmission of an explosion through an orifice, *Symp. Combust. Proc.*, 19 (1982) 599-606.

[7] G. Klingenberg, J.M. Heimerl, Gun Muzzle Blast and Flash, American Institute of Aeronautics and Astronautics, 1992.
[8] S. Lee, S. Kim, G. Lee, A Study on the Calculation of Muzzle Velocity Through the Gun Barrel Pressure Measurement, *J. Korean Soc. Propuls. Eng.*, 12 (2008) 60-66.
[9] Q. Qin, X. Zhang, Study on the Initiation Mechanism of Non-Premixed Shock Induced Combustion in Supersonic Propellant Gas Jet, *Propellants Explos. Pyrotech.*, 44 (2019) 1302-1311.
[10] K. Inaba, J. Shepherd, Plastic Deformation and Vibration in a Fluid-Filled Tube Subject to Axial Impact, *ASME Press. Vessels Pip. Conf.* (2009) 605-616.
[11] W. Vera-Tudela, C. Barro, K. Boulouchos, Investigations on spark pre-chamber ignition and subsequent turbulent jet main chamber ignition in a novel optically accessible test rig, *Int J Engine Res*, (2021) DOI: 10.1177/14680874211019849.
[12] S. Biswas, L. Qiao, Prechamber Hot Jet Ignition of Ultra-Lean H2/Air Mixtures: Effect of Supersonic Jets and Combustion Instability, *SAE International Journal of Engines*, 9 (2016) 1584-1592.
[13] Q. Malé, O. Vermorel, F. Ravet, T. Poinsot, Direct numerical simulations and models for hot burnt gases jet ignition, *Combust. Flame*, 223 (2021) 407-422.
[14] Q. Malé, O. Vermorel, F. Ravet, T. Poinsot, Jet ignition prediction in a zero-dimensional pre-chamber engine model, *Int J Engine Res*, (2021) DOI: 10.1177/14680874211015002.
[15] S. Biswas, S. Tanvir, H. Wang, L. Qiao, On ignition mechanisms of premixed CH 4 /air and H 2 /air using a hot turbulent jet generated by pre-chamber combustion, *Applied Thermal Engineering*, 106 (2016) 925-937.
[16] J. Tian, Z. Cui, Z. Ren, H. Tian, W. Long, Experimental study on jet ignition and combustion processes of natural gas, *Fuel*, 262 (2020).
[17] H. Phillips, Ignition in a transient turbulent jet of hot inert gas, *Combustion and Flame*, 19 (1972) 187-195.
[18] X. Tang, M. Asahara, A.K. Hayashi, N. Tsuboi, Numerical investigation of a high pressure hydrogen jet of 82 MPa with adaptive mesh refinement: The starting transient evolution and Mach disk stabilization, *Int. J. Hydrog. Energy*, 42 (2017) 7120-7134.
[19] R. Sadanandan, D. Markus, R. Schießl, U. Maas, J. Olofsson, H. Seyfried, M. Richter, M. Aldén, Detailed investigation of ignition by hot gas jets, *Pro. Combust. Inst.*, 31 (2007) 719-726.
[20] S. Coronel, J. Melguizo-Gavilanes, D. Davidenko, R. Mével, J. Shepherd, Reduction methodology for detailed kinetic mechanisms: application to n-hexane-air hot surface ignition, *11th Asia Pacific Combus. Conf.* (2017).